Acta Crystallographica Section B
Structural Science
ISSN 0108-7681

Molecular and crystal properties of *E*-1,2-bis(3-methoxy-2-thienyl)ethene: static disorder in the crystal

Frank Blockhuys,* Christophe M. L. Vande Velde, Stefan T. Maes, Carl Peten, Herman J. Geise, Christian Van Alsenoy and Albert T. H. Lenstra†

University of Antwerp, Department of Chemistry, Universiteitsplein 1, B-2610 Wilrijk (Antwerpen), Belgium

† Deceased 18 August 2002.

Correspondence e-mail: frank.blockhuys@ua.ac.be

Received 8 May 2003
Accepted 7 July 2003

The crystal structure of *E*-1,2-bis(3-methoxy-2-thienyl)ethene ($C_{12}H_{12}O_2S_2$) has been determined at five different temperatures, *i.e.* room temperature (293), 223, 173, 123 and 93 K. The solid-state work is complemented by the results of theoretical calculations of energies, geometries, difference electron densities and atomic charges of the free molecule. Analysis revealed static disorder caused by a higher energy conformer of the title compound, probably contaminating the crystal during its growth. The results support the contention that the electrical properties are mainly governed by the carbon backbone.

Dedicated to the memory of Professor Ab Lenstra – our colleague, teacher and friend.

1. Introduction

As part of our continuing research into the semiconductor applications of arylene vinylene oligomers (Tachelet *et al.*, 1994; Vanneste *et al.*, 1998; Poels *et al.*, 1998; De Wit *et al.*, 1998), we have synthesized various substituted 1,2-bis(2-thienyl)ethenes (Blockhuys *et al.*, 1999) in order to assess the influence of the pattern of substitution on the compounds' properties, amongst which are solubility and electrical conductivity. UV and electron spin resonance (ESR) spectroscopy indicate that the electronic properties of poly(thiophenes) and other poly(heterocycles) are dictated by the carbon backbone alone and that the role of the heteroatom is subordinate (Ford *et al.*, 1982; Tourillon, 1986). Preliminary investigations (Seus, 1965) had suggested similar behaviour for other heterocyclic arylenevinylene oligomers. A deformation electron density study, based on high-quality single-crystal X-ray diffraction intensities, is the ideal tool to gain information about the molecular π-systems of the latter type of compound and to test the suggestion above regarding similar behaviour. We selected the title compound, *E*-1,2-bis(3-methoxy-2-thienyl)ethene (Fig. 1), because the molecule has been successfully used in the synthesis of methoxy-substituted poly(2,5-thienylene vinylene) (PTV) derivatives (Blockhuys *et al.*, 1997, 2000) and can be taken as a model compound for PTV and other conjugated materials with interesting optical and electrical properties.

Unfortunately, it later became clear that the title compound suffers from disorder, jeopardizing our original aim of obtaining a high-quality experimental deformation electron density. Hence, to determine the electron density in the π-system we had to rely primarily on calculated electron densities. Fortunately, however, our efforts in collecting a large set of high-quality X-ray data at five different temperatures

allowed the identification of the disorder as being static and caused by the presence of *ca* 3% of a high-energy conformer (1*c*) along with *ca* 97% of the minimum-energy conformer (1*a*) (Fig. 1). Moreover, the results from Density Functional Theory calculations allowed the origin of the disorder to be better understood.

2. Experimental

The title compound was synthesized as previously reported (Blockhuys *et al.*, 1999) and single crystals were grown by the slow evaporation of solvent from a saturated solution in petroleum ether.

2.1. X-ray data collection

A red–brown crystal with an octahedral shape was mounted on an Enraf–Nonius CAD-4 diffractometer. The incident X-ray beam was produced with a fine-focus sealed Mo tube in combination with a graphite monochromator (UCAR-ZYA). Using a narrow vertical slit in front of the point detector, we estimated the crystal mosaicity at 1° in ω. The low-temperature measurements were achieved by cooling the crystal in the N_2 gas stream from an Enraf–Nonius FR558-NH cryostat. To avoid problems with icing, the diffractometer housing was sealed and the air inside was kept dry with silica gel. Cell dimensions, inferred from the angular settings of 25 reflections with $11 < \theta < 21°$, were measured at 10 K intervals between 293 and 93 K. The lengths of the three axes (in Å) as a function of temperature are given by

$$a(T) = 7.695 + 0.007T$$
$$b(T) = 11.526 + 0.006T$$
$$c(T) = 13.161 + 0.002T,$$

which show that the thermal expansion is clearly anisotropic. As can be seen from Fig. 2, there are no signs of discontinuities in any of the cell dimensions.

Reflection intensities were recorded in the $\omega/2\theta$ scan mode with a scan angle of $(1.3 + 0.7 \tan\theta)°$ and an aperture of $(2.7 + 0.4 \tan\theta)$ mm. Intensity data were corrected for a linear decay in intensity, which was detected *via* the intensity control reflections. Symmetry-independent reflections were collected at room temperature up to 0.7 $Å^{-1}$, while complete data sets were measured up to 1 $Å^{-1}$ at 223, 173, 123 and 93 K. Systematic absences uniquely indicated the space group *Pbca*. As we were using a point detector, we applied a measuring strategy designed to save time during the data collection: when the preliminary reflection scan resulted in a ratio for $I/\sigma(I) < 0.33$ no final scan of the reflection was carried out.

In addition to the conventional structure analysis (see below) additional symmetry and quality tests were performed. First, prior to each of the data collections we redetermined the unit cell in order to check for a possible phase transition which might be triggered by an ordering process in the solid state; no evidence for such a phase transition was found. Second, at 93 K, all intensities up to 0.64 $Å^{-1}$ were measured three times at azimuthal angles of −10, 0 and +10°. This small variation in ψ prevents significant fluctuations in reflection intensities caused by X-ray absorption. Merging the equivalent reflections, we arrived at an R_{int} value of 0.012. Moreover, the variation in ψ allowed us to detect and thus eliminate outliers caused by multiple scattering and in some cases to distinguish

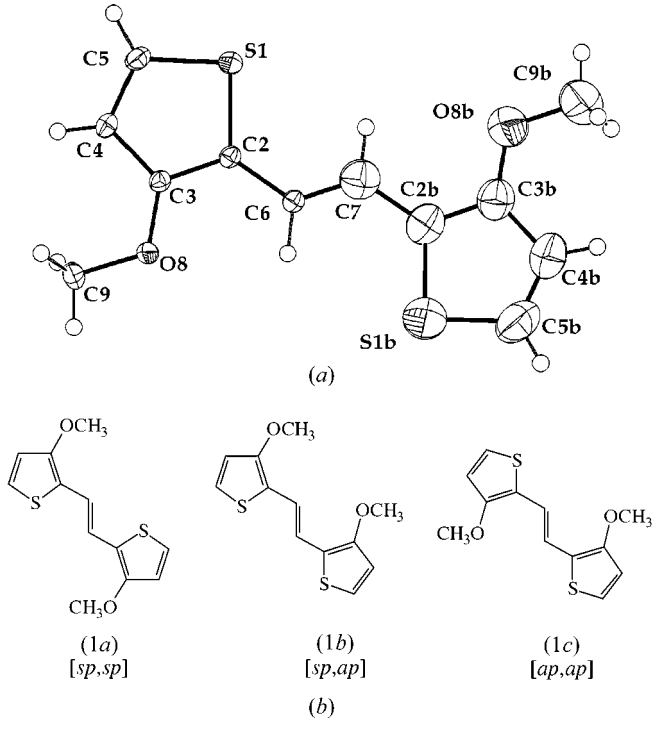

Figure 1
(*a*) Molecular structure and atomic numbering of [*sp*,*sp*]-*E*-1,2-bis(3-methoxy-2-thienyl)ethene (1*a*). XRD displacement ellipsoids (at 93 K on the left side of the molecule and at 293 K on the right side) are drawn at the 50% probability level and H atoms are shown as circles of small arbitrary radius. (*b*) The three planar conformers of *E*-1,2-bis(3-methoxy-2-thienyl)ethene and their IUPAC designations.

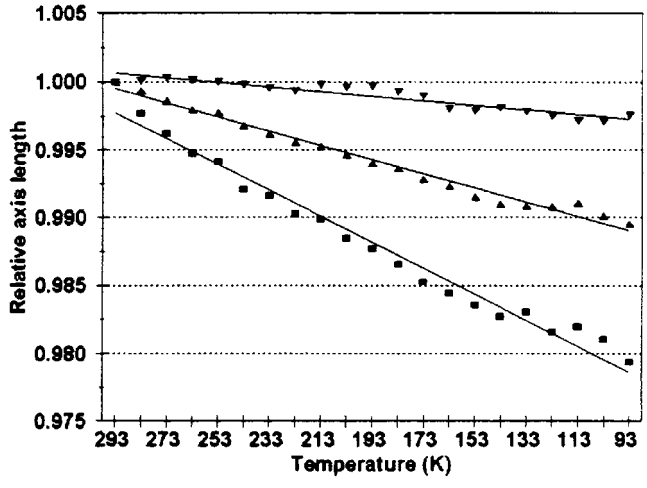

Figure 2
The variation in the *a* (squares), *b* (triangles) and *c* (inverted triangles) cell dimensions as a function of temperature.

Table 1
Experimental table.

Crystal data					
Chemical formula	$C_{12}H_{12}O_2S_2$				
Chemical formula weight (g mol^{-1})	252.4				
Cell setting	Orthorhombic				
Space group	*Pbca*				
Radiation type	Mo $K\alpha$				
Wavelength (Å)	0.71073				
Monochromator	Graphite				
Crystal form	Octahedral				
Crystal size (mm)	0.3 × 0.3 × 0.3				
Crystal colour	Red–brown				
No. of reflections for cell parameters	25				
θ range (°)	11–21				
F(000)	528				
T (K)	293	223	173	123	93
a (Å)	7.935 (1)	7.864 (1)	7.819 (1)	7.790 (1)	7.765 (2)
b (Å)	11.712 (1)	11.662 (1)	11.627 (1)	11.604 (2)	11.509 (2)
c (Å)	13.218 (1)	13.218 (1)	13.206 (1)	13.185 (2)	13.173 (2)
V (Å^3)	1228	1212	1200	1192	1186
Z	4	4	4	4	4
Z'	$\frac{1}{2}$	$\frac{1}{2}$	$\frac{1}{2}$	$\frac{1}{2}$	$\frac{1}{2}$
D_x (Mg m^{-3})	1.364	1.383	1.396	1.406	1.414
μ (mm^{-1})	0.42	0.42	0.43	0.43	0.43
Data collection					
Diffractometer	Enraf–Nonius CAD-4				
Data collection method	$\omega/2\theta$ scans				
No. of measured reflections (after merging)	1788	4981	4795	4890	4866
No. of observed reflections	1239	2010	2632	3286	3025
Criterion for observed reflections	$I > 2\sigma(I)$	$I > 2\sigma(I)$	$I > 2\sigma(I)$	$I > 2\sigma(I)$	$I > 2\sigma(I)$
$\theta_{max.}$ (°)	30	45	45	45	67
Range of h, k, l	$0 \rightarrow h \rightarrow 11$	$0 \rightarrow h \rightarrow 15$	$0 \rightarrow h \rightarrow 13$	$0 \rightarrow h \rightarrow 15$	$0 \rightarrow h \rightarrow 20$
	$0 \rightarrow k \rightarrow 16$	$0 \rightarrow k \rightarrow 23$	$0 \rightarrow k \rightarrow 23$	$0 \rightarrow k \rightarrow 22$	$0 \rightarrow k \rightarrow 29$
	$0 \rightarrow l \rightarrow 18$	$0 \rightarrow l \rightarrow 26$	$0 \rightarrow l \rightarrow 26$	$0 \rightarrow l \rightarrow 26$	$0 \rightarrow l \rightarrow 32$
No. of standard reflections	3	3	3	3	3
Frequency of standard reflections (h)	2	1	2	2	2
Intensity decay (%)	3.0	2.0	3.0	2.0	6.0
Refinement					
Refinement on	F^2	F^2	F^2	F^2	F^2
GOF	1.039	1.008	0.94	1.029	1.022
wR	0.149	0.174	0.191	0.134	0.152
R_u	0.049	0.056	0.055	0.046	0.049
R_{all}	0.089	0.153	0.116	0.081	0.089
No. of reflections used in refinement	1788	4980	4795	4890	4866
No. of parameters used	97	97	97	97	97
Weighting scheme	$w = 1/[\sigma^2(F_o^2) + (AP)^2 + BP]$, where $P = (F_o^2 + 2F_c^2)/3$				
A	0.07	0.07	0.09	0.06	0.07
B	0.21	0.15	0.61	0.25	0.41
$(\Delta/\sigma)_{max.}$	0.00	0.00	0.00	0.00	0.00
$\Delta\rho_{max.}$	0.26	0.35	0.058	1.16	0.89
$\Delta\rho_{min.}$	−0.23	−0.36	−0.05	−0.39	−0.33
Refinement with disordered molecule					
Refinement on	F^2	F^2	F^2	F^2	F^2
GOF	1.022	0.939	1.023	1.053	1.034
wR	0.115	0.143	0.205	0.108	0.127
R_u	0.045	0.052	0.053	0.038	0.042
R_{all}	0.086	0.153	0.116	0.075	0.083
No. of reflections used in refinement	1788	4980	4795	4890	4866
No. of parameters used	123	123	123	123	123
Weighting scheme	$w = 1/[\sigma^2(F_o^2) + (AP)^2 + BP]$, where $P = (F_o^2 + 2F_c^2)/3$				
A	0.04	0.04	0.11	0.05	0.05
B	0.38	0.38	0.08	0.09	0.26
$(\Delta/\sigma)_{max.}$	0.00	0.00	0.00	0.00	0.00
$\Delta\rho_{max.}$	0.19	0.27	0.59	0.48	0.43
$\Delta\rho_{min.}$	−0.24	−0.37	−0.54	−0.34	−0.33
S.O.F. 1a	0.964 (4)	0.972 (2)	0.9829 (18)	0.9701 (9)	0.9706 (10)
S.O.F. 1c	0.034 (4)	0.028 (2)	0.0171 (18)	0.0299 (9)	0.0294 (10)

Computer programs: *CAD*4 *Express* (Enraf–Nonius, 1994), *XCAD*4 (Harms & Wocadlo, 1996), *MolEN* (Fair, 1990), *SHELXL97* (Sheldrick, 1997), *PLATON* (Spek, 2003).

Table 2
Relative energies (in kJ mol^{-1}) of the three conformers of *E*-1,2-bis(3-methoxy-2-thienyl)ethene using different theoretical methods.

Conformer	Conformation	HF/6-31G*	B3LYP/6-31G*	B3LYP/6-311+G*
(1*a*)	[*sp*,*sp*]	0.00	0.00	0.00
(1*b*)	[*sp*,*ap*]	15.36	4.14	3.32
(1*c*)	[*ap*,ap]	11.18	6.82	5.18

multiple scattering from a change in crystallographic symmetry. The measurements on (001) illustrate this effect perfectly.[1] Third, the size of the 93 K data set was further increased from 0.64 to 1 Å^{-1} by measuring the additional reflections in a single scan with $\psi = 0^\circ$. Using our 123 K refined structural model we calculated the intensities for all independent reflections between 1.0 and 1.3 Å^{-1}. Those with an $|F_c|$ value larger than 1.5 were selected and subsequently measured.

The structure was solved using the Patterson and Fourier methods implemented in the *MolEN* software (Fair, 1990). For the refinement and crystallographic calculations the *SHELXL* software (Sheldrick, 1997) and *WinGX* program suite (Farrugia, 1999) were used. During the least-squares refinement individual reflections were weighted according to their errors, *via* the standard *SHELXL* weighting scheme. The results of the refinement are given in Table 1.

2.2. *Ab initio* calculations

The geometries of the three planar conformers of *E*-1,2-bis(3-methoxy-2-thienyl)ethane (Fig. 1) were calculated previously at the Hartree–Fock level (Blockhuys *et al.*, 1999). For this study full geometry optimizations were additionally performed for all conformers using *Gaussian*98 (Frisch *et al.*, 1998) at the DFT/B3LYP level of theory using the 6-31G* and 6–311+G* basis sets; these were used as they are implemented in the program. Force-field calculations at the B3LYP/6–311+G* level indicated that the conformations with a mirror plane through the heavy atom skeleton [(C_{2h} symmetry for (1*a*) and (1*c*) and C_s symmetry for (1*b*)] represent energy minima. Energy differences and IUPAC names of the three conformations are given in Table 2. The geometrical results of the calculations are presented in Table 3 for (1*a*); Cartesian coordinates for all conformers are given in the supplementary data.[2] Deformation densities were calculated by subtracting the pro-molecule density from the total molecular density, at the B3LYP/6–311+G* geometry. Stockholder charges were calculated as previously reported (Rousseau *et al.*, 2000), at the B3LYP/6–311+G* geometry.

3. Discussion

3.1. Discussion of the structure

An important result from the XRD analysis is that the title compound crystallizes (predominantly) in the [*sp*,*sp*] conformation (Fig. 1) – the calculations clearly indicate that this is indeed the lowest-energy conformer for the free molecule (see below). Values of bond distances and valence angles are listed in Table 3 as a function of the temperature for the experimental geometry; the B3LYP/6–311+G* geometry is given for comparison. An increase in temperature leads to an increase of the *intermolecular* distances, as is reflected in the behaviour of the cell axes, whereas it is clear from Table 3 that the *intramolecular* bond lengths in (1*a*) appear to decrease by an average of 0.01 Å for this 200 K temperature increase. The latter shrinkages are clearly due to libration. We used the experimental anisotropic displacement parameters (ADPs) as observations in the translation–libration–screw (TLS) analysis (Schomaker & Trueblood, 1968) implemented in *PLATON* (Spek, 2003). The molecular translation T proved to be almost isotropic and its behaviour harmonic: the mean-square displacements change from 0.052 Å^{-1} at 293 K to 0.017 Å^{-1} at 93 K. The centre of the molecule coincides with a crystallographic inversion centre and, consequently, the elements of the screw tensor are zero. The molecular libration L, on the other hand, is clearly anisotropic. The librational moment L_{11}, which is a rotation around the inertial axis along the long axis of the molecule, is one order of magnitude larger than the other two components. The mean square librational values for L_{11} are 37, 23, 17, 11 and 10 deg^2 at 293, 223, 173, 123 and 93 K, respectively. The libration L_{11} is thus the driving force behind the apparent bond shrinkages with increasing temperature. It also provides an explanation for the anisotropy in the thermal expansion along *a*, *b* and *c*. As mentioned before, the latter axis shows a minimal variation in relation to the temperature. As can be seen from Fig. 5, the long axis of the molecule follows approximately the crystallographic *c* direction; therefore, a temperature-induced change in L_{11} will have its main impact on the *a* and *b* axes.

The observed differences between the calculated geometries of the isolated molecule and the experimental solid-phase X-ray structures are expected and can be attributed to the differences between the definitions of $r_{\rm calc} \equiv r_e$ and $r_{\rm XRD} \simeq r_\alpha$ (Kuchitsu & Cyvin, 1972) or, as is the case with the change in

[1] Given the space-group symmetry, $I(001)$ should be zero, but at $\psi = 0^\circ$ we observed a rather intense reflection at the (001) position. However, measurements at $\psi = -10^\circ$ and $+10^\circ$ confirmed the systematic absence of (001). Fig. 3 shows the $\omega/2\theta$ plots of the 'forbidden' (001) reflection and of the allowed (002) reflection. The wavelength dispersion, which characterizes the incident X-ray beam, is found along the ω/θ diagonal in Fig. 3(*b*). Its absence in the (001) profile (Fig. 3*a*) emphasizes the non-standard nature of (001). The intensity of (001) as a function of ψ is depicted in Fig. 3(*b*): in this range of ψ a normal reflection such as (002) would be, and indeed was, independent of ψ. The clear *Umweganregung* of (001) at $\psi = 0^\circ$ is caused by two strong reflections of the crystal structure [$F(000) = 528$], *i.e.* the (210) reflection with $|F_c| = 144.6$ and (211) with $|F_c| = 103.7$. The observed structure amplitudes at $\psi = 0^\circ$ were 139.0 and 103.2, respectively. Thus, (210) shows an intensity loss of 10% at $\psi = 0^\circ$ due to Aufhellung. The (210) diffracted X-ray beams act as an incident X-ray beam for the (211) net planes, which causes a (211) reflection observed by us as (001). This scenario matches the geometrical prerequisite, *viz.* at $\psi = 0^\circ$, (001) and (210) coincide simultaneously with the Ewald sphere. That necessary condition for multiple scattering is easily negated by a small rotation in ψ, which is demonstrated in Fig. 4.

[2] Supplementary data for this paper are available from the IUCr electronic archives (Reference: BM5001). Services for accessing these data are described at the back of the journal.

Table 3
Experimental solid-state geometrical data at the five experimental temperatures (distances in Å and angles in °) and the B3LYP/6-311+G* calculated gas-phase molecular geometry (r_e in Å and angles in °) for (1*a*); only heavy atom data are given.

	293 K	223 K	173 K	123 K	93 K	B3LYP
S1—C2	1.729 (2)	1.7328 (12)	1.7313 (13)	1.7345 (8)	1.7349 (9)	1.7537
C2—C3	1.367 (3)	1.3740 (17)	1.3803 (17)	1.3798 (11)	1.3808 (12)	1.3871
C3—C4	1.418 (3)	1.4216 (16)	1.4208 (17)	1.4219 (11)	1.4235 (12)	1.4268
C4—C5	1.336 (4)	1.349 (2)	1.357 (2)	1.3600 (14)	1.3610 (14)	1.3660
C5—S1	1.712 (3)	1.7190 (16)	1.7184 (17)	1.7215 (11)	1.7212 (11)	1.7295
C2—C6	1.441 (3)	1.4419 (16)	1.4412 (17)	1.4416 (11)	1.4405 (12)	1.4383
C6—C7	1.328 (4)	1.341 (2)	1.347 (2)	1.3492 (16)	1.3493 (17)	1.3535
C3—O8	1.356 (2)	1.3571 (15)	1.3549 (16)	1.3581 (10)	1.3586 (11)	1.3627
O8—C9	1.414 (3)	1.4225 (17)	1.4272 (17)	1.4291 (11)	1.4297 (12)	1.4194
S1—C2—C3	109.39 (14)	109.48 (8)	109.57 (9)	109.62 (6)	109.55 (6)	109.54
C2—C3—C4	114.01 (19)	114.20 (11)	114.12 (12)	114.06 (8)	114.14 (8)	114.01
C3—C4—C5	112.1 (2)	111.82 (13)	111.71 (13)	111.92 (8)	111.79 (9)	112.16
C4—C5—S1	112.35 (19)	112.35 (10)	112.35 (11)	112.10 (7)	112.17 (7)	112.25
C5—S1—C2	92.12 (12)	92.15 (7)	92.25 (7)	92.30 (4)	92.35 (5)	92.04
S1—C2—C6	124.49 (16)	124.48 (9)	124.56 (10)	124.58 (6)	124.67 (7)	124.40
C2—C6—C7	126.7 (3)	126.28 (15)	125.95 (15)	125.96 (10)	125.87 (11)	126.74
C6—C2—C3	126.12 (19)	126.04 (11)	125.86 (11)	125.79 (7)	125.78 (8)	126.06
C2—C3—O8	118.94 (17)	118.97 (10)	118.93 (11)	119.08 (7)	119.01 (8)	119.65
C4—C3—O8	127.0 (2)	126.82 (12)	126.95 (12)	126.86 (8)	126.85 (8)	126.33
C3—O8—C9	117.64 (19)	116.92 (11)	116.50 (11)	116.29 (7)	116.07 (7)	117.74

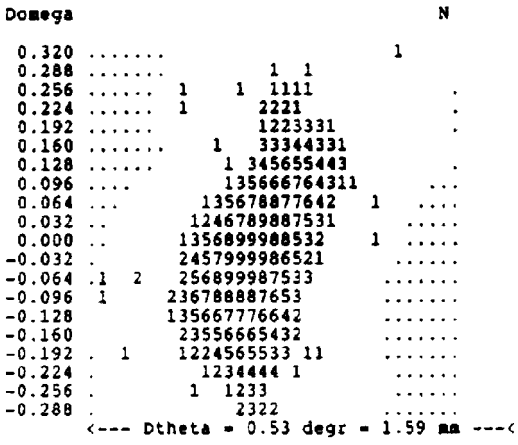

(*a*)

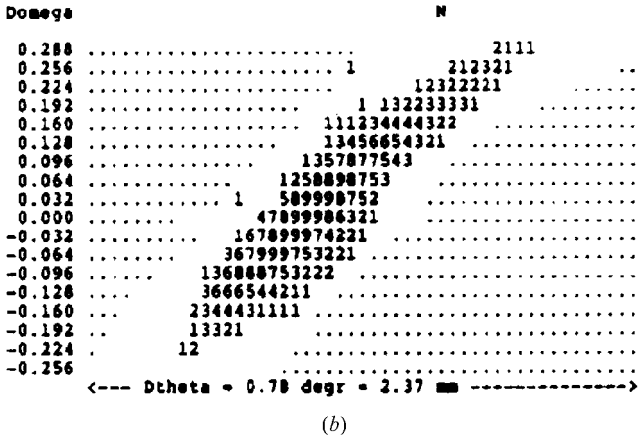

(*b*)

Figure 3
(*a*) $\omega/2\theta$ plot of the multiply scattered (001) reflection; (*b*) $\omega/2\theta$ plot of the normal (002) reflection.

molecular point group, to packing effects in the solid. The double–single C—C bond-length alternations, which are found in the experimental structure, are convincingly reproduced by the calculations, as are the differences between the two C—S bond lengths and the fact that the ethenediyl C═C bond length is the shortest of the C═C bonds.

3.2. Static disorder

We calculated a difference electron-density map exploiting the full set of intensity data from *E*-1,2-bis(3-methoxy-2-thienyl)ethene observed at 93 K. For a centrosymmetric structure, this distribution function should reveal details that are typical of a deformation map. When we subtract the crystallographic model, which consists of spherically

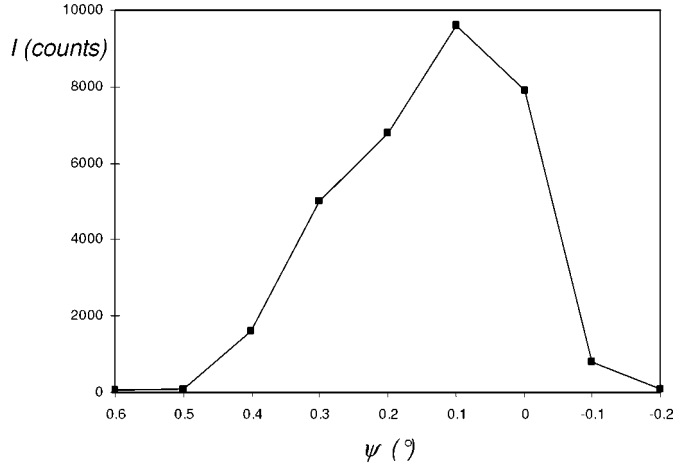

Figure 4
Azimuthal scan of the (001) reflection.

symmetric independent atoms, from the real molecular density, we would expect the effects of hybridization to become visible. The difference electron density in the plane of the molecule is presented in Fig. 6(*a*), where the molecule (1*a*) is also superimposed. Most characteristics in the difference map, such as the negative densities at atomic sites, are consistent with the concept of a deformation density, but some other elements are not. For example, the highest positive difference density feature is a peak lying close to the S atom; its position, displaced from both the line connecting the nuclear positions of the C and S atoms, and the bisector of the CSC angle, means that this maximum cannot be attributed to a C—S bond or a sulfur lone pair. Furthermore, the positive peak between C6 and C7 suggests a bond perpendicular to the existing one. Such features are incompatible with a deformation density and point towards a single cause, namely static disorder caused by an 'impurity' in the crystal lattice. We recall that the occurrence of disorder jeopardizes our initial objective, *i.e.* a good experimental electron-deformation density of the title compound. To avoid the loss of effort invested in the data collection we decided to investigate this disorder further. First, as detailed in §2.1, we scrutinized the unit-cell determinations at 93, 123, 173, 223 and 293 K to check for signs of a possible phase transition. No such sign, such as a discontinuity in the cell dimensions as a function of temperature or the appearance of 'forbidden' reflections, was observed. This begs the question as to which kind of disorder is present and which impurity causes it. In our opinion another conformer of the title compound, particularly conformer (1*c*) (Fig. 1), is present as the impurity in the crystal lattice. Several points lead to this conclusion.

The fact that conformer (1*b*) can be generated in two different ways (*i.e.* [*ap*,*sp*] formally differs from [*sp*,*ap*]), together with the results of the B3LYP/6-311G* calculations (Table 2), gives the equilibrium conformer composition at room temperature as (1*a*) (62%), (1*b*) (31%) and (1*c*) (7%). This seems to make (1*b*) the obvious candidate for the impurity. However, in contrast to (1*a*) and (1*c*), (1*b*) lacks an inversion centre and would therefore adopt a different symmetry. In fact, in *Pbca* with $Z = 4$, the (1*a*) molecules must be situated on inversion centres to produce the necessary eight symmetry independent residues, whereas (1*b*) molecules would be situated on general positions, resulting in $Z = 8$. The latter would show in the appearance of intensities $h + k$, $h + l$, $h + l = 2n$, which are forbidden in the former situation. Conformer (1*c*), on the other hand, differs from the major component (1*a*) only by the rotation of both thiophene rings by 180° around the C2—C6 and C2*b*—C7 bonds; (1*c*) also fits in the crystal lattice very well, as illustrated in Fig. 6(*b*). At the same time, we see from Fig. 6(*b*) that (1*a*) and (1*c*) have practically the same molecular shape and that the group dipoles of their (3-methoxy-2-thienyl) moieties remain well aligned in the crystal lattice. Steric demands and charge interactions being very similar, we conclude that the 'incorrect' incorporation of a (1*c*) molecule instead of a (1*a*) molecule can easily occur during crystal growth. Hence, we expect (1*b*) to be absent and (1*c*) to be the only contaminating species.

When we compare the peak height at the (1*a*) sulfur position in the Fourier map (51.33 e Å^{-3}) with the electron density at the highest difference peak (0.48 e Å^{-3}), we obtain a preliminary value of *ca* 1% for the amount of conformer (1*c*)

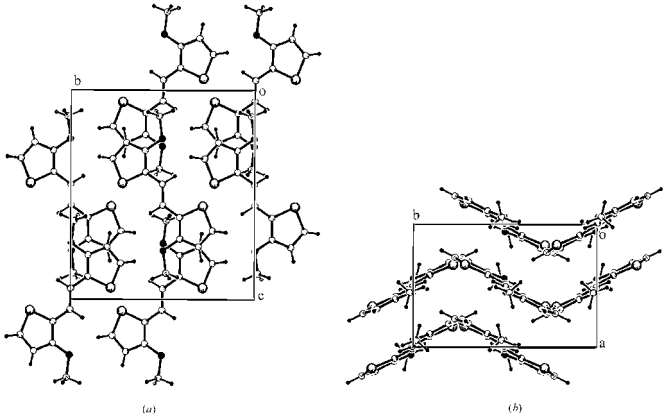

Figure 5
View of the crystal along the (*a*) *a* and (*b*) *c* axes.

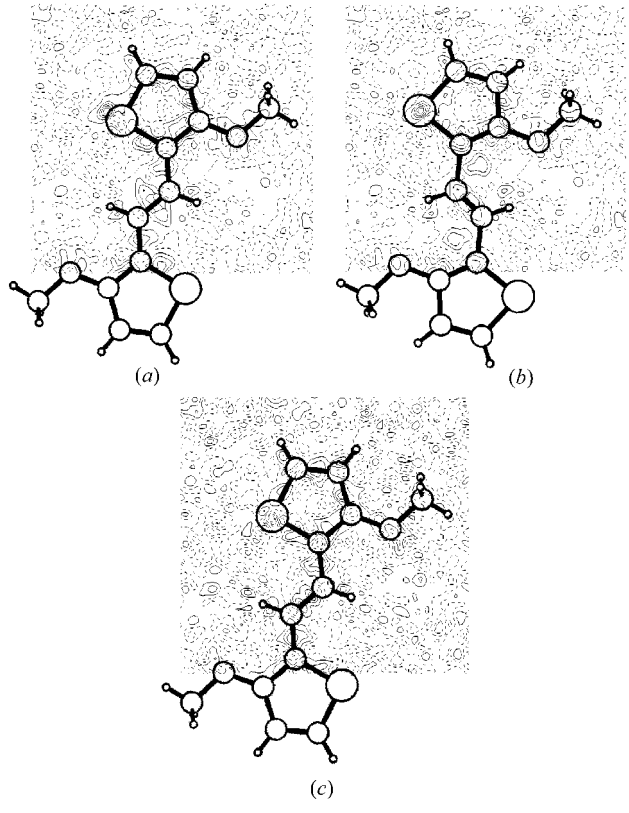

Figure 6
Experimental difference electron density maps of the 93 K data set (*a*) with the refined molecule [conformer (1*a*)] and (*b*) with the 'contaminant' conformer (1*c*) superimposed. (*c*) shows the difference map where the impurity in the crystal is taken into account in the refinement. Dotted lines indicate negative electron densities, full lines positive ones. The spacing between contour lines is 0.2 e Å^{-3}.

in the crystalline phase. An accurate estimate of that concentration is difficult to obtain in this manner, since we have to work close to the detection limits of the data set and the Fourier difference peak in question is affected by the presence of excess sulfur density at the adjacent (1*a*) position. However, refinement was possible after some simplifying assumptions, *viz.*:

(i) Rotation of the (3-methoxy-2-thienyl) moiety does not affect bond distances nor valence angles, and thus the distances and angles of conformer (1*c*) can be constrained to those of conformer (1*a*). The calculations indicate that the largest difference between (1*a*) and (1*c*) is 0.005 Å in bond lengths and 5.83° in angles; even though the latter is rather large, the effect on the overall molecular shape is limited.

(ii) The ADPs of the corresponding atoms in (1*a*) and (1*c*) are equal. In our analysis we fixed the ADPs of conformer (1*c*) to the corresponding values in (1*a*).

(iii) The conformers are coplanar and the central C═C bond in conformer (1*c*) is perpendicular to that in (1*a*).

We subsequently refined the crystal structure and the occupancies for the two conformers, applying flexible restraints to the interatomic 1,2- and 1,3-distances in the impurity, to match its geometry to the one of the major compound. This gave a stable refinement which converged with a model having 2.94 (10)% (1*c*) at 93 K. With $Z = 4$ this leads to three molecules of (1*c*) per 25 unit cells. This refinement was repeated for the data sets at the other temperatures. Table 1 shows that, at all temperatures, the addition of conformer (1*c*) to the structure with the constraints mentioned above, improves the various agreement indicators, diminishes the residual electron density and, most importantly, provides consistent results for the occupancy factor. Even though the latter differs by more than 3σ for the 173 K data set, the value is still of the same order of magnitude. The observation of a temperature-independent contamination level points to static disorder and is compatible with the suggested pollution during crystal growth.

To further investigate the latter issue, we compare the calculated relative energies of the three conformers (Table 2). Assuming that the calculated energy levels allow a reliable estimation of the relative abundances of the conformers in the apolar solvent petroleum ether, the table shows that the solution contains significant amounts of all three conformers. Applying the Boltzmann distribution law to the energy differences obtained from the B3LYP/6–311+G* calculations, and taking into account that conformer (1*b*) can be generated in two different ways (*i.e.* by rotation of either of the two thiophene rings), the calculations predict that such a solution would contain a mixture consisting of 62% (1*a*), 31% (1*b*) and 7% (1*c*), as was mentioned above. This means that there is a 9:1 abundance of (1*a*) with respect to (1*c*), disregarding solvent effects which are negligible in this case. Allowing for the absence of conformer (1*b*) in the solid state (see above), we conclude that the relative abundance of the conformers in solution is roughly comparable with their abundance in the crystal. This indicates that the two conformers are sufficiently similar that their incorporation kinetics into a crystal of (1*a*) are likewise roughly equivalent. Thus, the abundance of (1*a*) and (1*c*) in the crystal reflects the equilibrium in solution.

Finally, we note that the calculations using different methodologies demonstrate a conspicuous switching of the energy order on going from the HF to the DFT calculations: conformer (1*b*), which is the least stable according to HF, has switched places with conformer (1*c*), making it the least stable. Intuitively, as well as on the basis of the level of theory and the size of the basis set used, one expects the latter situation to be true. It has been suggested that in conformer (1*a*) two intramolecular hydrogen interactions exist between an H atom of the ethenediyl spacer and the O atom of the methoxy group in a stable five-membered ring configuration, designated CH—*n*(O) (Blockhuys *et al.*, 1999). On going from conformer (1*a*) to (1*b*) only one of these interactions needs to be broken, while both are broken on going from (1*a*) to (1*c*). Since breaking such an interaction destabilizes the conformer, it is logical that conformer (1*c*) is destabilized by about twice the amount as (1*b*), as can be seen from Table 2. We conclude that in its description of *E*-1,2-bis(3-methoxy-2-thienyl)ethene the HF calculation does not take sufficient account of the effect of the CH—*n*(O) interaction.

3.3. Deformation densities

An unfortunate consequence of the static disorder found in the crystal phase of (1*a*) is that no conclusive evidence can be obtained from the experimental data regarding either the

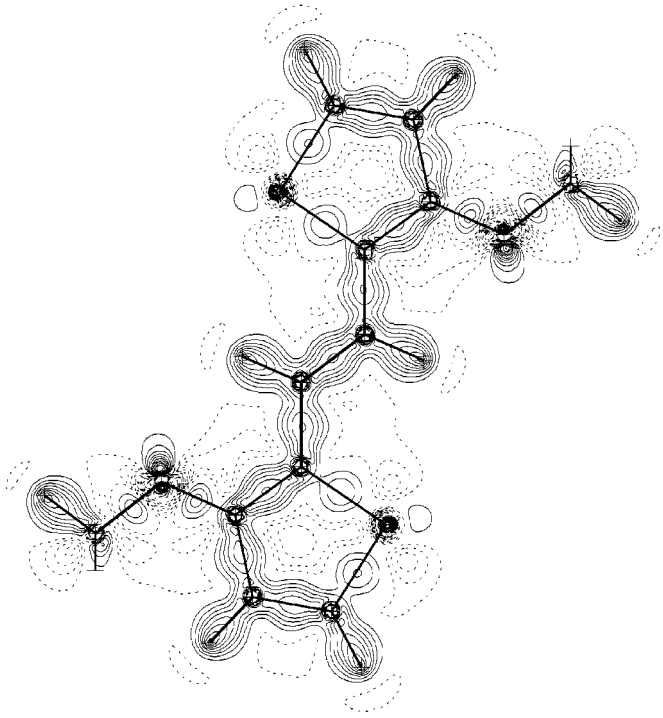

Figure 7
Calculated deformation electron density of [*sp*,*sp*]-*E*-1,2-bis(3-methoxy-2-thienyl)ethene (1*a*). Full lines indicate positive electron density, dashed lines negative electron density. Positive isodensity lines were plotted every 0.1 e Å^{-3}, in the range 0–2.3 e Å^{-3}, and negative ones every 0.05 e Å^{-3}, in the range from 0 to −1.00 e Å^{-3}.

Table 4
Calculated stockholder charges (in *e*) for [*sp*,*sp*]-*E*-1,2-bis(3-methoxy-2-thienyl)ethene (1*a*).

Atom	Charge
S1	0.068
C2	−0.050
C3	0.045
C4	−0.084
C5	−0.072
C6	−0.058
O8	−0.117
C9	0.002
H4	0.048
H5	0.056
H6	0.040
H91	0.037
H92	0.037
H93	0.049

carbon-backbone-based conductivity of these types of compounds or the existence of the aforementioned CH$-n$(O) interaction. We have, however, included as Fig. 6(*c*) a final electron difference-density map which, although distorted by the inclusion of the 2.94 (10)% of the conformer (1*c*), provides an approximate view of the electron deformation density in the molecule. One feature which is especially worth noting is that the electron density in the sulfur–carbon bonds is lower than that in the carbon–carbon bonds, especially C2—C6 and C3—C4. The bond between C6 and C7 appears to be split into two peaks and the lone pairs of oxygen are hardly visible, both of which can be attributed to the slightly overestimated occupancy factors of the disordered molecule.

A more elegant solution regarding the carbon-backbone-based conductivity was found in the deformation densities obtained from the theoretical calculations. Since there were no unusual discrepancies between theoretical and experimental geometries, we assumed that the theoretical deformation density would be an accurate representation of the experimental one. This can be seen from a comparison of Figs. 6(*c*) and 7. Furthermore, the calculated deformation densities have the advantage that the effects of the crystal field and the observed disorder cannot introduce distortions. Fig. 7 shows the deformation density of (1*a*) in the plane of the heavy atoms. In contrast to Fig. 6, Fig. 7 gives a clear picture of the distribution of electrons in (1*a*) and shows that most of the negative charge is indeed located in the carbon-atom skeleton. The electron density in the various C—C bonds is two to three times higher than in the C—S bonds, while the C—O bonds also show a reduced electron density. The largest overall density is still found in the electron lone pairs of the O atoms; those on the S atoms have all but disappeared. These findings are confirmed by the results of the calculation of the stockholder charges on the atoms; these are given in Table 4. While the positive charge on sulfur and the large negative charge on oxygen are striking, all the C atoms, except the methyl carbon and C3 bearing the methoxy group, bear large negative charges. The large positive charge on C3 is explained by the large inductive electron-accepting (−*I*) effect of the O atom. The charge on the methyl C9 atom is virtually zero, which is somewhat surprising, taking the difference density plot into account. Nevertheless, Fig. 7 visually confirms that the bulk of the electron density is located in the carbon backbone, which strengthens the idea that the electrical properties of this and related materials are dictated by the length, conformation and configuration of the carbon backbone and that the role of the sulfur or other heteroatom is subordinate.

4. Conclusions

A definitive molecular and crystal structure is presented for [*sp*,*sp*]-*E*-1,2-bis(3-methoxy-2-thienyl)ethene at five different temperatures. The low-temperature measurement presents clear evidence for the existence of static disorder in the solid state due to the presence of a high-energy conformer of the title compound. The results of high-level theoretical calculations provide geometrical and energetic data on the different conformers of the compound, enabling a better understanding of the precise causes of the disorder. Furthermore, they provide additional data regarding the distribution of the electrons in the compound through calculated difference-density maps and stockholder charges on the atoms.

SM thanks the Flemish Institute for Science and Technology, IWT, for a predoctoral scholarship. CVV thanks the Fund for Scientific Research, FWO-Vlaanderen, for a grant as research assistant. FB and CVA gratefully acknowledge support by the University of Antwerp under Grant GOA-BOF-UA No. 23.

References

Blockhuys, F., Claes, M., Van Grieken, R. & Geise, H. J. (2000). *Anal. Chem.* **72**, 3366–3368.
Blockhuys, F., Hoefnagels, R., Peten, C., Van Alsenoy, C. & Geise, H. J. (1999). *J. Mol. Struct.* **485–486**, 87–96.
Blockhuys, F., Peten, C., De Wit, M. & Geise, H. J. (1997). *Synth. Met.* **84**, 347–348.
De Wit, M., Vanneste, E., Geise, H. J. & Nagels, L. J. (1998). *Sens. Actuators B*, **50**, 164–172.
Enraf–Nonius (1994). *CAD*4 *Express*. Version 5.1/1.2. Enraf–Nonius, Delft, The Netherlands.
Fair, C. K. (1990). *MolEN*. Enraf–Nonius, Delft, The Netherlands.
Farrugia, L. G. (1999). *J. Appl. Cryst.* **32**, 837–838.
Ford, W. K., Duke, C. B. & Salaneck, W. R. (1982). *J. Chem. Phys.* **77**, 5030–5039.
Frisch, M. J., Trucks, G. W., Schlegel, H. B., Scuseria, G. E., Robb, M. A., Cheeseman, J. R., Zakrzewski, V. G., Montgomery, J. A. Jr, Stratmann, R. E., Burant, J. C., Dapprich, S., Millam, J. M., Daniels, A. D., Kudin, K. N., Strain, M. C., Farkas, O., Tomasi, J., Barone, V., Cossi, M., Cammi, R., Mennucci, B., Pomelli, C., Adamo, C., Clifford, S., Ochterski, J., Petersson, G. A., Ayala, P. Y., Cui, Q., Morokuma, K., Malick, D. K., Rabuck, A. D., Raghavachari, K., Foresman, J. B., Cioslowski, J., Ortiz, J. V., Baboul, A. G., Stefanov, B. B., Liu, G., Liashenko, A., Piskorz, P., Komaromi, I., Gomperts, R., Martin, R. L., Fox, D. J., Keith, T., Al-Laham, M. A., Peng, C. Y., Nanayakkara, A., Gonzalez, C., Challacombe, M., Gill, P. M. W., Johnson, B., Chen, W., Wong, M. W., Andres, J. L., Gonzalez, C., Head-Gordon, M., Replogle, E. S., & Pople, J. A. (1998). *Gaussian*98, Revision A.7. Gaussian, Inc., Pittsburgh PA.
Harms, K. & Wocadlo, S. (1996). *XCAD*4. University of Marburg, Germany.

Kuchitsu, K. & Cyvin, S. J. (1972). *Molecular Structures and Vibrations*, edited by S. J. Cyvin, ch. 12. Amsterdam: Elsevier.
Poels, I., Nagels, L. J., Verreyt, G. & Geise, H. J. (1998). *Anal. Chim. Acta*, **370**, 105–113.
Rousseau, B., Peeters, A. & Van Alsenoy, C. (2000). *Chem. Phys. Lett.* **324**, 189–194.
Schomaker, V. & Trueblood K. N. (1968). *Acta Cryst.* B**24**, 63–76.
Seus, E. J. (1965). *J. Heterocycl. Chem.* **8**, 318–320.
Sheldrick, G. M. (1997). *SHELX*97. University of Göttingen, Germany.
Spek, A. L. (2003). *PLATON*. Utrecht University, The Netherlands.
Tachelet, W., Jacobs, S., Ndayikengurukiye, H., Geise, H. J. & Grüner, J. (1994). *Appl. Phys. Lett.* **64**, 2364–2366.
Tourillon, G. (1986). *Handbook of Conducting Polymers*, edited by T. A. Skotheim, Vol. 1, p. 293. New York: Marcel Dekker, Inc.
Vanneste, E., De Wit, M., Eyckmans, K. & Geise, H. J. (1998). *Semin. Food Anal.* **3**, 107–113.